Developing a thermal atlas for climate-responsive urban design based on empirical modeling and urban morphological analysis

Feng Yang [a,b], Liang Chen [c,*]

[a] College of Architecture and Urban Planning (CAUP), Tongji University, Shanghai, China
[b] Key Laboratory of Ecology and Energy-Saving Study of Dense Habitat, Tongji University, Ministry of Education, China
[c] School of Geographic Sciences, East China Normal University, Shanghai, China

ARTICLE INFO

ABSTRACT

This paper aims at developing a thermal atlas system at the urban district scale to evaluate the urban thermal environment and identify thermally vulnerable areas. Shanghai Lujiazui Central Business District was selected as a test bed for the method. Six key morphological indicators, i.e., sky view factor, pavement cover ratio, vehicle traffic density, green plot ratio, frontal area index and proximity to heat sink were used to describe different aspects of the urban thermal environment including building density, land use, anthropogenic heat, greenery, ventilation potential and heat sink. Spatial analysis tools were developed in geographical information system to generate maps for these morphological indicators. In situ meteorological measurements were carried out on peak summer days to investigate the spatial variation of microclimatic parameters, based on which the physiological equivalent temperature (PET) index was calculated. Empirical regression models were built correlating PET values with local morphological indicators, based on which PET maps were generated. This thermal atlas system can rapidly analyze and visualize the spatial variations of urban microclimate from the thermal comfort aspects as affected by different urban design scenarios, thus can be a useful decision-support tool for urban design towards alleviating urban heat island intensity and improving outdoor thermal comfort.

1. Introduction

Urban climate has notable impacts on building energy use, outdoor thermal comfort and air quality. To architects and urban designers, the urban climate at the urban district or neighborhood scale (10^{-2}–10^3 m, as estimated by Oke [1]), or microclimate, is of utmost interest, as it could be manipulated by design interventions: building form, height and spacing, pavement and façade materials, street parks and trees, etc. [2]. Designers normally make environmental judgment based on their perception of the region, city and site, as well as their knowledge and experiences. Nowadays, as cities keep growing larger and denser, designers are constantly faced with the challenges of working in high-density and high-heterogeneity urban environment. In such a case, tools are in great need to help designers gain a better microclimatic understanding by providing predictive results for different design scenarios with acceptable accuracy and validity. The commonly employed tools are based on computational fluid dynamics (CFD) [3]. CFD tools require expertise to operate, are generally resource-costly, and thus unfamiliar and not user-friendly to architects and urban designers. On the other hand, at the urban scale, urban climatic mapping (UC-Map) is a design decision support tool that aims to provide urban planners with both analytical and visual information [4]. It has received increasing attention from both research and practice fields over the last decade. Studies have been carried out in a number of cities in Europe, North America and Asia. Among them, the project commissioned by the German government is the first effort in integrating and legitimating the climate information into urban planning process. On the metropolitan and urban scale, the urban form-based variables are generally categorized into two layers of Thermal Load and Dynamic Potential; regional wind information was also provided [5]. The established framework has been applied in various cities in Germany, and has influenced the paradigms used in subsequent UC-Map studies and applications across the world [6,7].

Earlier UC-Maps generally stratify climate information based on land use, and rely largely on expert evaluation. A more recent UC-Map in Hong Kong factors building density, topography, ground roughness and greenery into street-level urban microclimate evaluation [8], and a systematic and quantitative approach is taken,

* Corresponding author. Tel.: +862154341246; fax: +862154341131.
  E-mail address: lchen@des.ecnu.edu.cn (L. Chen).

List of Nomenclature and abbreviations

ψ_{sky}	sky view factor
Ψ	transmissivity
λ_p	pavement Cover Ratio
λ_t	vehicle Traffic Density
λ_g	green Plot Ratio
af(z)	frontal Area Density
λ_{hs}	proximity to Heat Sink
BCR	building Cover Ratio
H/W	aspect Ratio
UHI	urban Heat Island
PET	physiological Equivalent Temperature
GSR	global Solar Radiation
Ta	air temperature
RH	relative humidity
WD	wind direction
WV	wind velocity
TZ	thermal zone

using urban morphological variables such as sky view factor (SVF) and frontal area density (FAD) to describe thermal and aerodynamic characteristics of high-density Hong Kong urban environment [9].

Our previous work indicates that thermal variations at pedestrian level can be well explained by empirical models built upon carefully-selected urban morphological variables [10,11]. The empirical modeling method takes a more quantitative approach with considerations of micro-scale urban design parameters, therefore is expected to be supplementary to the state-of-the-art UC-Map systems by providing pertinent implications for design strategies.

This study aims at developing a thermal atlas system that is suitable for Shanghai's unique urban characteristics and climatic conditions, and is easy to use in urban design practice. The two key questions to be answered are: (1) How to define the set of urban morphological parameters that contribute significantly to the microclimatic differentials in a high-rise, high-density urban environment and (2) How to map such spatial differentials with respect to thermal comfort gradient, based on morphological understandings. In order to answer these questions, this study takes an integrated approach which combines geographic information system (GIS)-based modeling and on-site meteorological measurement. The Lujiazui central business district (CBD) in downtown Shanghai is used as a case study.

2. Methodology

2.1. Study area

Shanghai (30°40′N—31°53′N, 120°51′E—122°12′E), the biggest city in China, is located on the alluvial terrace of the Yangtze River delta with average elevation of 4 m above sea level. It has a northern subtropical monsoon climate, with a mean annual temperature of 17.2 °C, and monthly mean maximum temperature of 30.2 °C in July and monthly mean minimum temperature of 1.9 °C in January, respectively. The city's administrative boundaries cover a total terrestrial area of 6340.5 km^2 excluding estuary waters. The city has a total population of 24.15 million, including both permanent and non-permanent residents [12]. The Lujiazui CBD is located in the Pudong New District on the eastern bank of Huangpu River just across the Bund. The total land area is 1.7 km^2, and covers commerce, business and high-end residential land uses. The total building floor area is about 4.35×10^6 m^2, and the gross floor area ratio about 2.5. With totally more than 40 super high-rise buildings (building height >200 m), Lujiazui (LJZ) CBD is considered as one of the most important financial hubs in China, and its planning and design has strong influences on the development practice of other Chinese cities. It is therefore selected as the case study area. Fig. 1 shows the map of LJZ CBD and its digital elevation model (DEM).

2.2. Identifying critical morphological parameters

This study adopts the morphometric methods to establish empirical relationships between urban form and microclimate. Various spatial indicators have been defined in urban climatological studies to characterize the urban morphology and its thermodynamic and aerodynamic properties, for instance, the SVF and the aspect ratio (building height to street width, H/W) of a street canyon are related to the radiation balance and airflow pattern [13], the building cover ratio (BCR, building footprint area to plot area) is related to roughness length (Z_0) and thus pollutant dispersion [13,14], etc. As the urbanization process modifies the
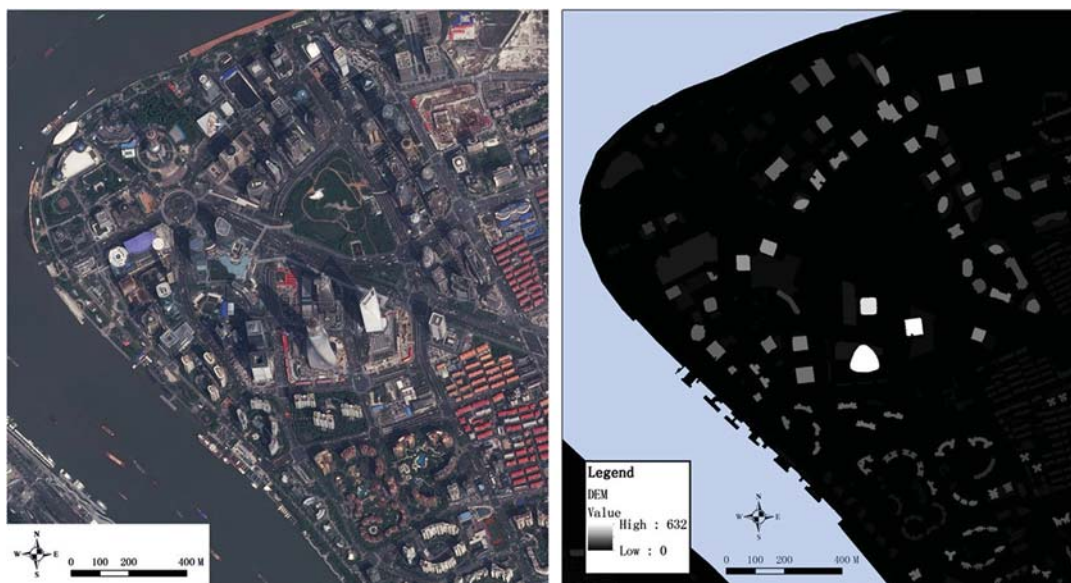

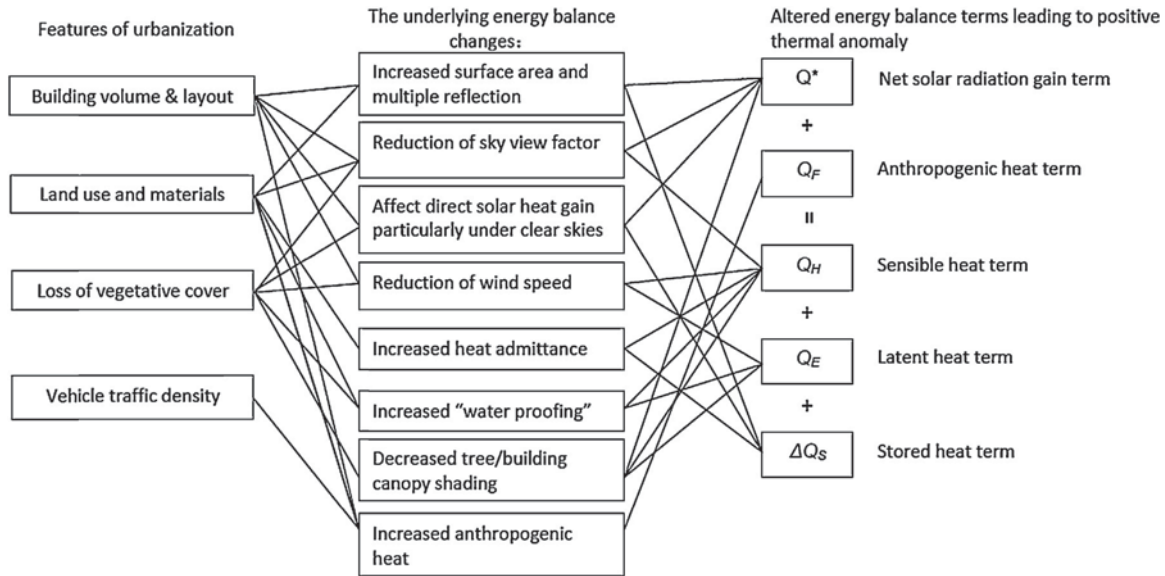**Fig. 1.** (a) Map of Lujiazui CBD in Shanghai (b) DEM.

Fig. 2. Interconnection among urbanization, morphology and urban energy balance (after Oke [1], pp. 275, 294)

morphological characteristics of the urban substrate in various ways which significantly alter the urban energy budget and lead to positive thermal anomaly [1], it is necessary to take a comprehensive account of involved design parameters in order to understand the impact of design interventions on the urban microclimate. Fig. 2 gives a conceptual framework of the interconnections among urbanization, underlying urban energy balance changes and resultant thermal anomaly.

The present study aims at building such interconnections through a quantitative approach and mapping outdoor human thermal comfort in dense urban areas. At the urban district and neighborhood scale, the fundamental principle of thermodynamics and aerodynamics are still valid, but the parameterization of urban form should adapt to the micro-scale, and the contributions from each parameter should be weighted with reasonable degrees of scientific rigor. The study follows the framework of Thermal Load and Dynamic Potential, but classifies the urban microclimatic characteristics into six categories, i.e., building form/density, land use/cover, anthropogenic heat, vegetation cooling, ventilation potential and proximity to heat sink. Key morphological variables are identified for each category based on the previous work of authors and a systematic review on the state of the art in urban climatology and urban morphometry. The variable set is listed

in Table 1. The following section provides introductions to the selected morphological variables and the scientific basis of their roles in affecting the urban microclimate.

2.2.1. Sky View Factor (ψ_{sky})

Dense urban areas tend to reduce the long-wave radiative heat loss to the sky as a heat sink at night, which is a major contributor to the formation of urban heat island (UHI). During the daytime, however, streets and outdoor places in dense urban area tend to be cooler than low-density area, due to protection from solar radiation by surrounding buildings or trees. The effect of urban form and density on daytime outdoor thermal condition is largely determined by the relationship between urban geometry and solar components (direct normal and diffuse). Due to high humidity and cloud cover in Shanghai, the diffusive component is a major one in the total horizontal solar radiation [21]. Therefore the degree of openness to the sky is related to solar admittance. Variables that can be used include SVF and H/W. The case study area of Lujiazui CBD featuring an urban form of interspersed high-rise buildings with large area of open spaces, therefore SVF is more suitable than H/W, and is selected in this study. Previous research shows that SVF is negatively correlated with maximum nocturnal urban–rural temperature differential [22]. On the other hand, during hot

Table 1
Morphological variable set.

	Categories	Morphological variables	Definition	Refs.
Thermal load	Building form and density	Sky view factor (ψ_{sky})	Ratio between the radiation received by a planar surface from the sky to the radiation emitted to the entire hemispheric radiating environment: Solar admittance in daytime and irradiative cooling at night. *Tree canopy is considered.*	[15]
	Land use/cover	Pavement cover ratio (λ_p)	Ratio of total impervious pavement area to the 50-m-radius area centered by the measurement point	[16]
	Anthropogenic heat	Vehicle traffic density(λ_t)	VTD = Sum((1/distance)*length)Function of distance to a road and the road length: the effect of vehicle traffic heat emission	[17]
Cooling potential	Vegetation cooling	Green plot ratio (λ_g)	Ratio of total leaf area to the 50-m-radius area centered by the measurement point: green mass and leaf density	[18]
	Ventilation potential	Frontal Area Density (af(z))	A measure of the frontal area per unit horizontal area per unit height increment: quantify the drag force as a function of building height.	[19]
	Proximity to heat sink	Proximity to Heat Sink (λ_{hs})	The distance to the centroid of any nearby sizable water body and green space	[20]

summer days, the sign of correlation can be either positive or negative depending on different density of the urban environment [4,23,24], which again confirms the complexity of daytime intra-urban temperature differences.

2.2.2. Pavement Cover Ratio (λ_p)

Paved and impervious urban surface generally absorbs more solar heat during daytime and consequently releases more at night as compared to vegetated surface, which contributes to UHI formation. Consequently the ratio of paved area is an effective indicator for describing imperviousness of land cover. Surface surveys using grey-level photography were conducted and results showed that the majority of pavement materials used in Lujiazui are impervious and in mid-to-light grey color within a narrow albedo range. Our previous study on high-rise residential quarters in Shanghai also suggests that albedo is not a significant influencing factor for air temperature differences at pedestrian level [10]. Therefore, only PCR is considered in this study. The use of 50-m-radius areal average is adopted as suggested by [16,25].

2.2.3. Frontal area density ($af(z)$)

The effect of building geometry on pedestrian-level wind velocity modification needs to be parameterized. Variables used to estimate surface roughness length (Z_0) include BCR [14] and $af(z)$ [9]. For the urban form of dense high-rise buildings with heterogeneous heights, FAI is more suitable than BCR as it can provide three-dimensional information of the building geometry, and is therefore selected for the study.

2.2.4. Vehicle traffic density(λ_t)

Anthropogenic heat is an important contributor to urban warming. In a CBD area, primary sources for anthropogenic heat emission are heat from heating, ventilation and air-conditioning (HVAC) systems and heat induced by vehicle traffic. In Lujiazui CBD, most outdoor parts of HVAC systems (air outlet, condensing tower, etc.) are installed on podium level and service-floors of main towers, therefore the effect of the emitted heat on pedestrian level is not significant. So only heat induced by vehicle traffic is taken into account. VTD is developed for this aspect, considering road network hierarchy and distance to road centers.

2.2.5. Green plot ratio (λ_g)

Vegetated surface modifies microclimate by evapotranspiration and shading. A two-dimensional index such as green space ratio is not sufficient in quantifying the comprehensive thermal effect of green mass. This study uses the green plot ratio, invented by Ong, which measures the overall leaf density of a given urban area [18].

2.2.6. Proximity to heat sink (λ_{hs})

Water bodies and green spaces are important heat sinks that can alleviate the adverse thermal effect of urbanization. The proximity to heat sink is dependent on the shape and size of the heat sink, the distance to it and the angle between prevailing wind direction. The two prominent heat sinks within the Lujiazui CBD are Huangpu River and Lujiazui Central Green (LCG). Because Huangpu River is to the leeward side (northwest) of Lujiazui CBD while LCG is to the windward side, therefore LCG is chosen as the heat sink, and PHS is calculated considering wind direction and distance to the centroid of LCG (in the artificial lake in LCG).

2.3. Thermal comfort assessment

The biometeorological index of physiological equivalent temperature (PET) is used to assess the overall effect of the local microclimatic condition on human thermal comfort. PET is a temperature scale (in °C) index that enables the assessment of the thermal components of climates based on personal experience [26]. It is defined as "the air temperature at which, in a typical indoor setting, the heat balance of a human body is maintained with core and skin temperatures equal to those under the conditions to assess". By definition, PET builds a linkage between the comprehensive influence of the complex outdoor climatic environment on thermal comfort and the thermal experience indoor, which can be easily estimated based on intuition and common sense. In addition, the temperature scale makes it easy to be interpreted by individuals without domain knowledge in physiology or meteorology, which makes it commonly accepted among designers and planners. Originated in mid-high latitude Germany, PET has been applied in a number of thermal comfort studies in different climates including hot–humid (sub-) tropical regions, e.g., Taiwan [27] and Hong Kong [28].

2.4. Meteorological measurement

Summertime field measurement campaigns were carried out on 29th and 30th, July 2013, in order to quantify the relationship between urban micrometeorological variables and urban morphological variables. A fixed weather station was installed at 1.5 m above ground level in the open lawn of the LCG, continuously recording wind velocity (WV), wind direction (WD), air temperature (Ta), relative humidity (RH) and global solar radiation (GSR) at a 10 s interval. Two-day synchronized traverse measurements were carried out along pre-selected routes. Each route links nine measurement points, started from the LCG and ended at the waterfront area. A tailor-made portable weather tracker was carried by two research assistants, measuring WV, WD, Ta, RH and globe temperature (Tg) at the 10 s interval, for 10 min at each point, and each measurement measured two rounds per day, i.e., one in the morning from 8:30 AM to 10:45 AM, and one in the afternoon from 15:00 PM to 17:15 PM. The 10 min means of each meteorological parameter are used as measured values of each round. The instrument specifications are listed in Table 2. The measurement totally covers six routes with 54 measurement points, as shown in Fig. 3.

In particular, the mean radiant temperature (Tmrt) was calculated using Ta, RH, WV and Tg according to the methods suggested by [29]. The selected thermal comfort index PET was calculated using Ta, RH, WV and Tmrt, and assuming constant metabolism rate of 80 W and cloth levels of 0.9 clo [26].

2.5. Morphological modeling and mapping

A set of GIS-based spatial analysis tools were developed to calculate and map the critical morphological parameters using geo database, including digital elevation model (DEM) and other urban information databases such as land use, building info, greenery, road network. This section gives a brief introduction to the modeling methods.

2.5.1. Sky view factor (ψ_{sky})

The sky view factor (ψ_{sky}) method developed by [4] was extended by considering the effect of vegetation. Two additional DEMs were used, which are the vegetation height, and the trunk height. In reality, it is very rare that a tree behind a tall building can still obstruct the sky, therefore this extreme case was neglected in this study. The spatial relation given by [30] was adopted, but using DEM for fast processing. Fig. 4 gives an illustration of different objects that obstruct the sky along a certain direction from a given point, including: tree (T1) with the lowest trunk elevation angle ($\angle 1$); tree (T2) with the highest elevation angle ($\angle 2$), its trunk elevation angle ($\angle 3$); and building (B) with the highest elevation angle ($\angle 4$) [31].

Table 2
Instruments specification.

Model	Parameter	Accuracy	Operating Range
Temperature/RH Smart Sensor: Hobo S-THB-M002	Ta, RH	±0.2 °C (0–50 °C); ±2.5% RH (10–90%)	−40 °C–75 °C; RH ≤95%
Wind direction smart sensors: Hobo S-WDA-M003 (on the fixed station only)	WD	±3% (17–30 m/s); ±4% (30–44 m/s) WV; ±5° (WD)	0–44 m/s WV0–355° (WD)
Wind velocity sensor: Cambridge Accusense sensor T-DCI-F900-S-P	WV	±5% of reading or ±0.05 m/s (15–35 °C)	0–10 m/s
Temperature smart sensor: S-TMB-M002 (installed in a 40 mm matt-grey vinyl ball)	Tg	±0.2 °C (0–50 °C)	−40–100 °C
Global radiation sensor: Hobo S-LIB-M003 (on the fixed station only)	GSR	±2% at 45° from vertical	0–1280 W/m² (300–1100 nm)

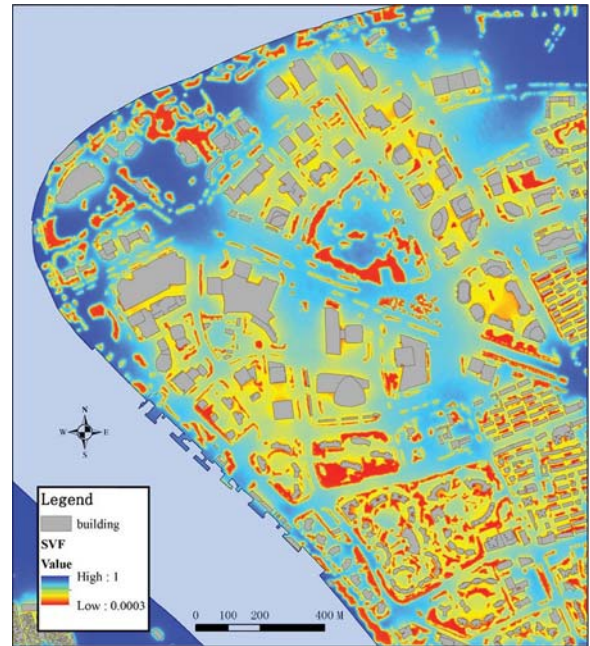**Fig. 3.** Map of Lujiazui CBD showing the traverse and fixed stations.

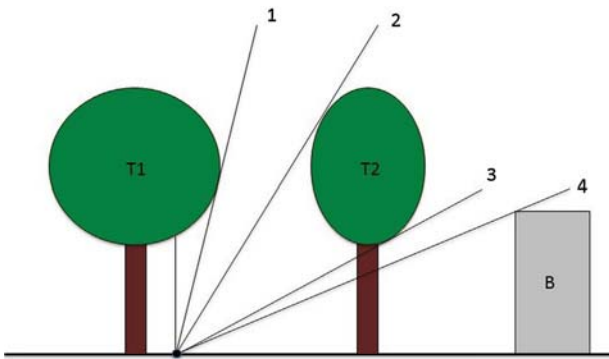**Fig. 5.** SVF map for the study area.

Fig. 4. Elevation angle for different objects that obstruct the sky along a certain direction.

Base on the above spatial configuration, the sky-view factor for the given point can be given as:

$$\psi_{sky} = 1 - \psi_{(B)} - \psi_{(T1)} \bullet (1 - \psi_{(T2)}) \bullet (1 - \psi) \tag{1}$$

where, $\psi_{(B)}$, $\psi_{(T1)}$ and $\psi_{(T2)}$ are the view factors of B, T1 and T2 respectively. Ψ is the transmissivity for trees, indicating the transparency of tree crown. In practice the value of 0.03 was selected for shortwave radiation [32]. Following the raster-based method in [4], the calculation for $\psi_{(B)}$, $\psi_{(T1)}$ and $\psi_{(T2)}$ individually was fairly straightforward. For a rotation angle of a (indicating a given direction):

$$\psi_{(B)} = \sin^2(\angle 4) \bullet a/360 \tag{2}$$

$$\psi_{(T1)} = \sin^2(90°) \bullet a/360 - \sin^2(\angle 1) \bullet a/360 \tag{3}$$

$$\psi_{(T2)} = \sin^2(\angle 2) \bullet a/360 - \sin^2(\angle 3) \bullet a/360 \tag{4}$$

And different bigger/smaller relationship between the four elevation angles need to be checked to ensure there is no re-calculating of obstructed sky, e.g., if $\angle 4$ is bigger than $\angle 2$ then there will be no additional obstruction to the sky caused by T2. Different elevation angle scenarios were analyzed, and the raster-based method can process the comparison fairly fast. The SVF map for the study area is shown in Fig. 5. The performance of the developed model was quite good: on a daily used PC with 3.20 GHz CPU, 4 GB memory, the model calculates the SVF of the study area (1 km by 1 km with 2 m resolution) within 1 h.

The simulated SVF values at measurement points are correlated fairly well with values calculated based on hemispherical sky view images, which were calculated using SOWEIG 1D software [32] (Fig. 6). The discrepancy could be attributed to the fact that the photographic method does not consider the transmittance of tree canopies, i.e., they are considered zero of transmissivity, which will cause underestimation of SVF.
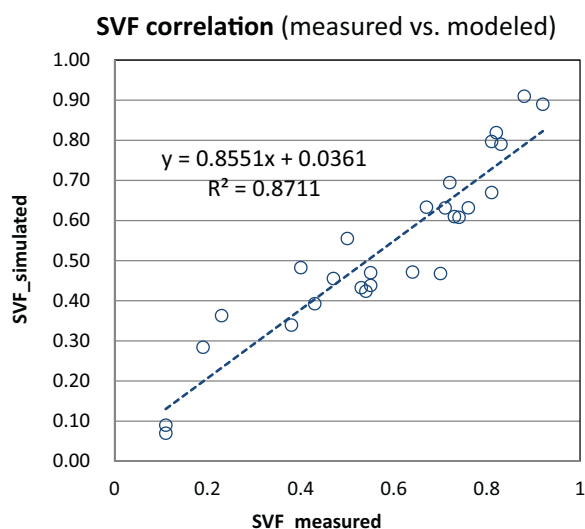
SVF correlation (measured vs. modeled)

Fig. 6. correlation of measured SVF with modeled SVF.

2.5.2. Green plot ratio (λ_g)

The green plot ratio(λ_g) was calculated based on the definition given in [18], which is the average leaf area index (LAI) value on a surface. The typical LAI values proposed by [18] were selected, i.e., 1.0 for grass, 2.0 for shrub, and 5.0 for trees. Standard GIS functions were used based on DEM data for the calculation.

2.5.3. Pavement cover ratio (λ_p)

Pavement cover ratio (λ_p) is also calculated with standard GIS functions. Land use dataset was used to determine if a pixel is paved or not.

2.5.4. Frontal area density (af(z))

The GIS based tool developed in [19] was used to calculate the af(z) map with

$$a_f(z, \theta) = A(\theta)_{proj}/(\Delta z)(A_T \bullet \Delta z) \tag{5}$$

where, $A(\theta)_{proj(\Delta Z)}$ is the area of building surfaces projected into the plane normal to the approaching wind direction for a specified height increment Δz; θ is the wind direction angle; and A_T is the total plan area of the study site. The algorithm reads in the wind rose data and derives the total af(z) for a site by calculating the weighted summation of the af(z) for all wind directions.

2.5.5. Vehicle traffic density(λ_t)

A GIS-embedded extension was developed to model the heat induced by road traffic. In practice the λ_T is influenced by various factors, and related heat emission is very difficult to predict. This study takes a simplified approach by using the road network to estimate the vehicle traffic and related heat emission. The preliminary assumptions are that the length and width of road segment will have a proportional relationship withλ_T, and the distance to a road segment will have a reverse proportional relationship withλ_T. In this case, λ_t for a given point is defined as:

$$\lambda_t = \sum (L(i)/D(i)) \tag{6}$$

where, $L(i)$ is the length of the ith road segment, and $D(i)$ is the distance from the given point to this road segment. The algorithm iterates through all road segments and calculates the summation of theλ_T.

2.5.6. Proximity to heat sink (λ_{hs})

λ_{hs} is calculated using standard GIS Euclidean distance function, which calculates the distance from the given point to the centroid of the water body in Lujiazui park to be considered as heat sink.

3. Results and analysis

3.1. Meteorological measurement result

The traverse and fixed measurement points are shown in Fig. 3. The meteorological conditions during measurement period are plotted in Fig. 7. The weather conditions in the two days are fairly similar, partially cloudy and hot and humid. The prevailing winds show a clear southeastern pattern, and an overall weak wind environment at pedestrian level.

Site photos, hemispherical sky images and meteorological data profiles of measurement points along Route A are shown in Fig. 8. It can be seen that the temperature variation, particularly the globe temperature (Tg), was largely affected by the degree of openness to the sky. For instance, the tree-shaded point A5 was remarkably cooler than adjacent locations. The air temperature (Ta) was even lower than the reference LCG station during both morning and afternoon measurement sessions because of the dense tree shading; Tg has decreased approaching Ta, indicating improved thermal comfort compared to points under higher degrees of solar exposure.

3.2. Empirical modeling

The measured ψ_{sky} showed positive correlation with PET: it can explain more than 50% of the variations in PET (Fig. 9), which confirms that ψ_{sky} is an important influencer of thermal comfort. On the other hand, ground material did not show a decisive impact on the local thermal condition: for instance, a point over grass lawn (A8) was hotter than the next point over a paved waterfront esplanade (A9).

The empirical datasets are divided into two groups: modeling group and validation group. Each group has 27 measurement points. The empirical modeling process was carried out based on the modeling group datasets. Pearson correlation and linear-fit regression were carried out among the thermal indices PET, six morphological variables (Table 1), and three control variables, namely Ta_cg, Vw_cg and SR_cg which are air temperature, wind velocity and solar radiation at the reference LCG station, respectively. The result indicates that, among the six morphological variables, PET is significantly related with ψ_{sky}, λ_g, af(z) and λ_{hs} at 0.01 significance level (two-tailed), and related with HPR at 0.05 level (two-tailed). For the control variables, PET is only significantly related to Ta_cg at 0.05 level (two-tailed). A nonparametric correlation test (Spearman's rho) reveals similar results.

The analysis also reveals that λ_t is insignificant in the correlation. We speculate that this is probably because λ_t is assumed to map the spatial distribution of traffic-induced waste heat during a relatively longer period, whereas the measurements only captured the heat from nearby vehicles during short periods (i.e., 10 min). In this sense, long-term measurements with fixed weather stations are likely to better measure the impact of λ_t, on the other hand vehicle-counting could be an alternative for a short-term measurement, as suggested in [33]. This has to be considered in future work to improve the experiment design.

When building a multiple-linear regression model, one must check the potential collinearity problem among independent variables. In this case, ψ_{sky} is found to be significantly correlated with af(z), λ_p and λ_g. The negative correlations of ψ_{sky} with af(z) and λ_g are reasonable, as increasing area of building facade generally
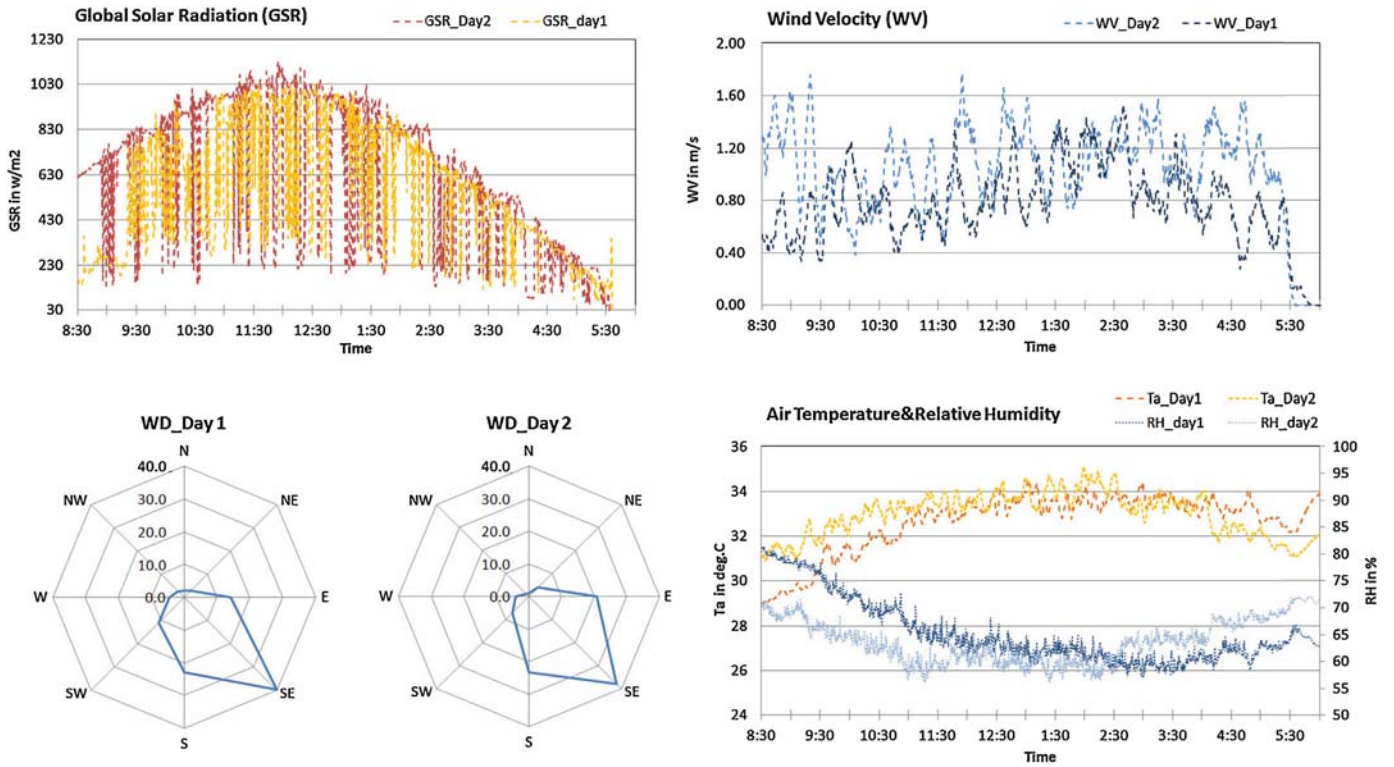
Fig. 7. Meteorological conditions measured at Lujiazui Central Green (LCG) station (Day1: 29 July, Dday2: 30 July).
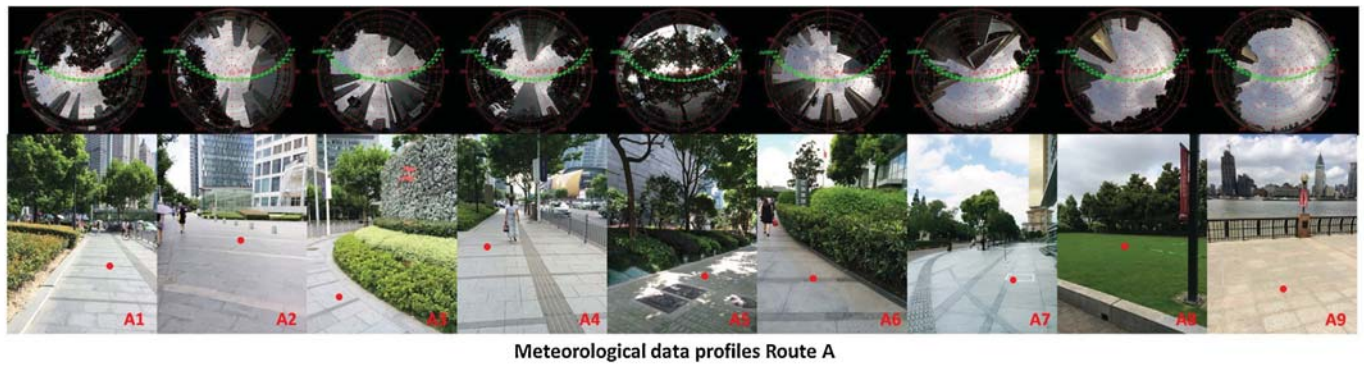

Fig. 8. SVI and site images of measured points on Route A and meteorological data profiles.

SVF(measured) vs. PET

$$y = 0.0583x - 1.644$$
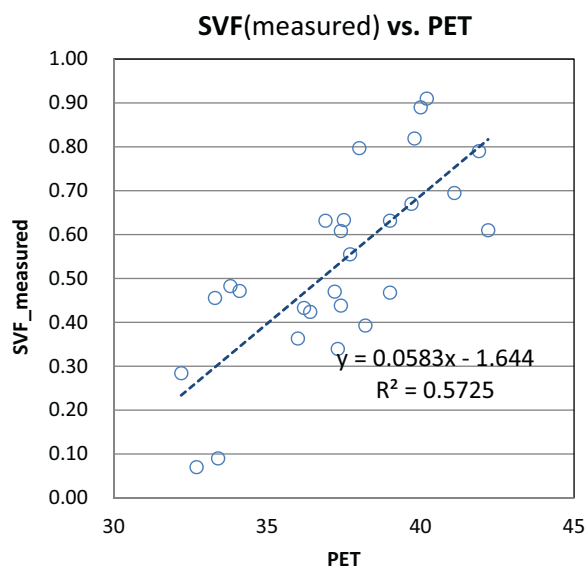$$R^2 = 0.5725$$

Fig. 9. Correlation of measured SVF with PET (sample size: 27).

reduces the viewable sky accordingly, and increasing coverage of vegetation, especially trees reduces it as well. The negative correlation occurring between ψ_{sky} and λ_p could be attributed to the measurement points with lower ψ_{sky} that are generally located between tall commercial buildings where the ground surface tends to be impervious (roads, sidewalks and parking lots, etc.), whereas those with higher ψ_{sky} are mostly located within or close to open spaces (small parks or waterfront greenery) and consequently less hard surfaces are found around them.

With the collinearity effect in mind, regression analysis was carried out including all the six morphological variables and one control variable (i.e., Ta_cg). Significant variables were firstly all entered to obtain a model with all sub-layers of variables and with the highest explanation power. Less important variables were then removed (Stepwise, Backward and Forward Methods), in order to build a parsimonious model that keeps the key variables while retaining the highest possible explanatory power. The result is as follows (Eqs. (7) and (8)).

$$PET = 8.51 + 0.81 \cdot Ta\_cg + 3.66 \cdot \psi_{sky} - 0.31 \cdot \lambda_p - 1.07 \cdot \lambda_g$$
$$- 4.13 \cdot af(z) + 0.004 \cdot \lambda_{hs} \qquad \otimes \ (7)$$
$$(R^2 = 0.79)$$

$$PET = -48.33 + 2.58 \cdot Ta\_cg + 7.42 \cdot \psi_{sky} - 0.93 \cdot \lambda_g$$
$$(R^2 = 0.76) \qquad (8)$$

3.3. Verification and validation of the empirical models

The validation group is used to test the validity of the models. The PET values calculated using field-measured data are plotted against modeled PET values. The scatter plots and linear-fit estimations are shown in Fig. 10. The linear estimation fits fairly well, and Eq. (8) shows a higher explanatory power (∼0.64) than that of Eq. (7) (∼0.54). This is reasonable, because considering the limited sample size, the simpler model with less independent variables (Eq. (8)) is more robust (with F statistics = 23.6) than the model with all important variables (Eq. (7), with F statistics = 10.3). The validity of the built model in explaining thermal comfort level with morphological variables is therefore confirmed.

3.4. Generating the thermal atlas

The morphological sub-layers were generated, as shown in Fig. 11. The PET maps were then generated based on the sub-layers and the empirical modeling results. The reference air temperature (Ta_cg) is set as a constant, using daytime mean Ta of 32.1 °C during the measurement period at LCG station. Fig. 12 shows the PET maps generated based on the two regression results.

The PET mapping is synthesized using the raster function in GIS, and the contributions from respective variables are weighted based on the regression coefficients. According to the range of PET values, six classes are assigned referring to the ranges of PET for different grades of thermal comfort perception and thermal stress given by [34], Class 1 and 2 can be categorized as warm, Class 3–5 as hot, and Class 6 as very hot.

The PET map indicates that, in the summer days with microclimatic conditions similar with the measurement period (Fig. 7), the overall thermal condition in LJZ Shanghai can be ranging from warm to hot. The spatial variations of PET are mainly due to the differences of building density and layout, vegetation and proximity to heat sink.

The warm area (class 1 and 2) is mainly distributed in densely vegetated area, i.e., LCG, Lujiazui Waterfront Park and several high-end housing quarters at the southern LJZ area. Smaller patches exist around commercial buildings, due to the low SVF caused by building shading. The street blocks to the north side of LCG primarily fall into class 2, with some part in class 1, which can be attributed to shading of buildings and street trees, and adjacency to the heat sink, i.e., LCG at their windward side. The local thermal stress level is moderate, indicating walkable outdoor spaces during the day.

On the other hand, the hot and very hot areas (Class 3–6) are normally found at wide roads, open grass lawn, and paved plazas. In particular, the area in the northeast of the investigated area is found to have the most severe heat stress. In fact it is a construction site (as can be seen from Fig. 1), therefore the very hot condition is largely caused by high levels of ψ_{sky} and λ_p, and low level of λ_g. The updated morphological and land cover information should be added to generate new PET maps when the construction is completed to re-analyze and re-evaluate that area.

4. Design implication and future work

Urban planning and design practices always strive to strike a balance among many issues and requirements from political, economic, social as well as environmental aspects. In this case study, LJZ CBD is one of the most prestigious financial hubs and tourist attractions in China. Therefore the planning and design of LJZ CBD should give emphasis on making comfortable outdoor spaces which can benefit hundreds of thousands of office commuters and tourists everyday. Unlike in mid-latitude cities with temperate climate, the sub-tropical climate of Shanghai requires that the summertime cooling issue is more important than wintertime heating. The generated summertime thermal comfort map in this study should be revealing to designers, policy makers and all stakeholders, as it provides clear visual information on outdoor thermal comfort levels, as well as its relationships with urban morphological variables which can be altered and controlled by design intervention. To simplify the hierarchy system and highlight the most important information, we generate a thermal zoning map based on PET map (Fig. 13) and identify three thermal zones (TZs) in Table 3.

Judged from the thermal zoning map, three aspects are worth design consideration for improving the local thermal comfort condition:
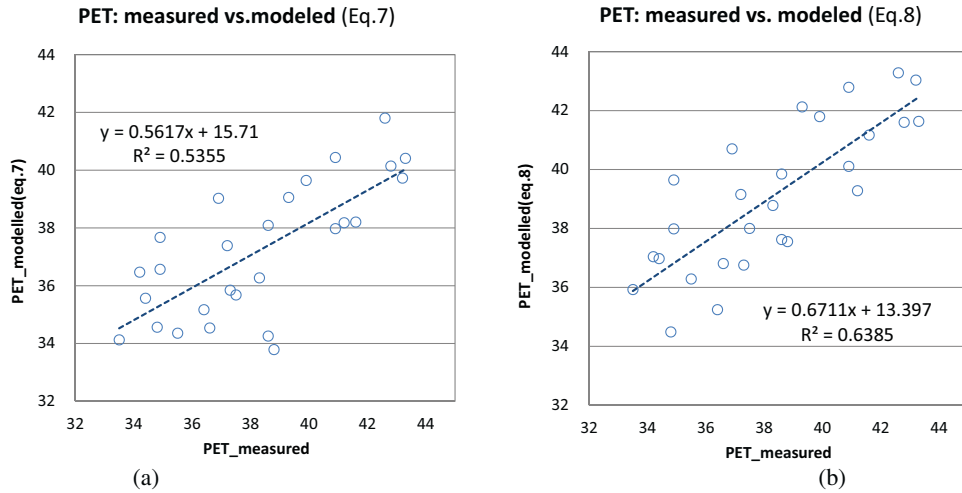
PET: measured vs.modeled (Eq.7)

(a)

PET: measured vs. modeled (Eq.8)

(b)

Fig. 10. Linear fit of field-measured PET with modeled PET (a) using Eq. (7), and (b) using Eq. (8).

(a) SVF

(b) GPR

(c) PCR

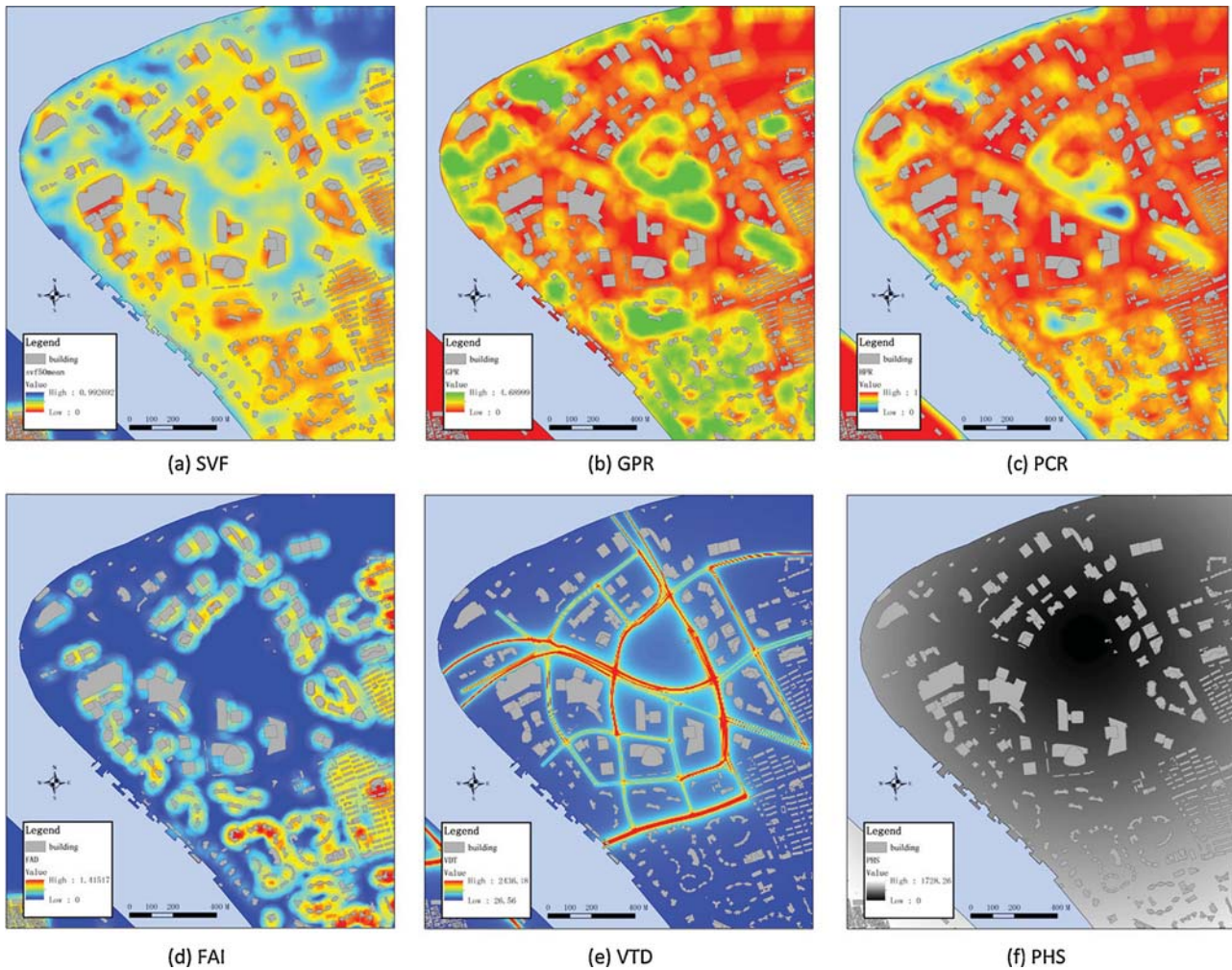(d) FAI

(e) VTD

(f) PHS

Fig. 11. Six morphological sub-layers (50 m radius average).

(1) Providing opaque shading devices for major pedestrian spaces at century walkways and waterfront esplanade. These two areas are highlighted in Thermal Zone 1, i.e., the most thermally vulnerable areas. Both places are designed for pedestrians and are intensively used by tourists and office commuters, but currently without any effective shading devices or tree cover. To add sun

protection at these places will be the most effective measure that can immediately improve summer daytime thermal comfort.

(2) Reducing the size of street blocks, and dividing massive single buildings into building clusters with smaller spacing. It can observed from Fig. 13, that the street blocks with smaller sizes
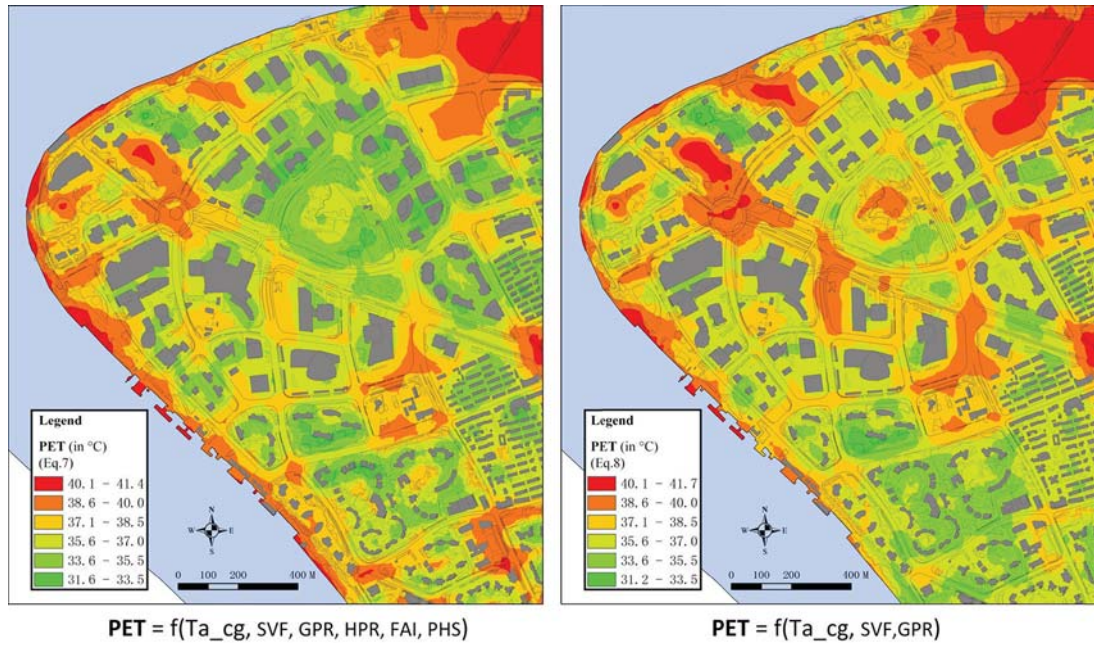
$$PET = f(Ta\_cg, SVF, GPR, HPR, FAI, PHS)$$ $$PET = f(Ta\_cg, SVF, GPR)$$

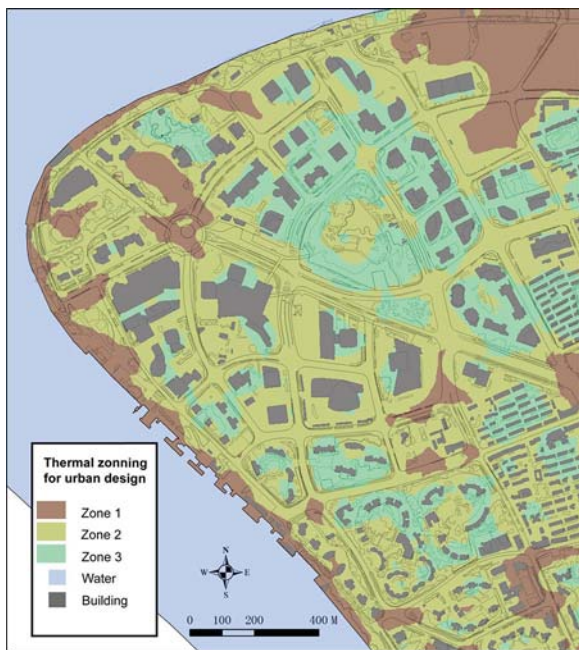**Fig. 12.** Summer daytime thermal atlas of Shanghai Lujiazui CBD (index: PET).

Fig. 13. Thermal zoning map based on PET maps.

and building clusters with smaller footprint (but closer to each other) are significantly cooler than the larger street blocks with a single and massive building. This is because denser urban fabric creates shaded outdoor spaces between buildings, whereas isolated super-tall or super-large buildings generally occupy larger street blocks (typically >400 m for each side of the block), and are separated by wide roads. This leads to uncomfortable pedestrian environment, because of less solar protection, and more sensible heat from nearby road pavement materials. Refining the urban grid and building fabric to a scale of 150–250 m not only improve daytime thermal comfort, but also make the city more walkable and thus more pedestrian-friendly.

(3) Improving the accessibility to the prominent heat sinks. For instance, expanding the existing walkway system to improve the connection between surrounding office buildings with LCG, so as to increase the occupation and usage of LCG during lunch hours and weekend days; designing building and landscape elements carefully, for instance, by reorganizing short walls, trees etc., so as to introduce more cool breeze from LCG to its surrounding built-up areas. Also, overly-wide roads such as the Century Avenue in Lujiazui CBD (100 m in width) should be avoided, because on the one hand, it is very pedestrian unfriendly; on the other, the street blocks on the southwest side of the Century Avenue could enjoy better cooling effect from LCG with a narrower road with lower heat capacity.

Table 3
Thermal zoning based on the PET map.

Thermal zones and features	Urban morphological characteristics	Measures for improvement
TZ1: extremely vulnerable to heat stress	Open area with little obstruction to sky, lowest vegetation coverage: paved waterfront; construction site; parking lots; major road intersections.	Provide shading (man-made canopy or tree cover where appropriate); increase vegetation coverage; enhance proximity to heat sink.
TZ2: high density and high usage space	large street blocks; massive buildings with large footprint; large building spacing; grass lawn with no tree coverage; major roads and pavements	Reduce the street block scale; replace large single buildings with smaller and adjacent buildings to create shadowed space and wind path; increase vegetation coverage.
TZ3: climatic valuable area	Green space with dense tree cover, e.g., LCG and waterfront park; residential quarters with dense vegetation; tall buildings with small spacing and smaller street blocks.	Maintain and improve.

The present study tested the methodology of combining empirical modeling and spatial analysis techniques in creating a thermal atlas system at the urban district scale. This thermal atlas system comprises the following components: urban morphological maps (or sub-layers), empirical models based on field-measured data (for sub-layer weighting and model validation), derived thermal comfort indices maps (PET in this case), and thermal zoning and design recommendation maps.

To better support climate-responsive urban design for various climate conditions, more work is needed in the future. Firstly, night-time and wintertime data need to be incorporated in empirical modeling, so that the urban morphological effect on microclimate and thermal comfort for different time and seasons can be evaluated comprehensively. This is particularly important for the high-rise high-density urban forms (such as the Lujiazui CBD) in a hot-summer and cold-winter climate zone. Secondly, the current framework is primarily based on the energy balance of urban surface. In future study the influence of meso-scale climate on the aerodynamics of the urban environment, such as regional wind information based on meso-scale wind simulation or urban observatory databases, should be added as an additional sub-layer for providing better understanding of urban ventilation.

5. Conclusion

This paper presents a thermal atlas system developed for supporting climate-responsive urban design under the sub-tropical climate of Shanghai. The system is based on empirical modeling and GIS-based spatial analysis by DEM modeling. Carefully selected morphological variables and control variables have been shown to be able to explain nearly 80% of the variability in the thermal comfort index of PET. The morphological variables were then calculated and mapped in the virtual urban space, and a thermal atlas was generated by overlaying the key morphological variable layers based on the coefficients determined by the empirical models. A set of PET maps is thus generated, and verified against field-measured data. A thermal zoning map is derived from the PET maps, based on which design recommendations can be suggested.

To our best knowledge, the present study is the first attempt to combine empirical modeling with GIS-based spatial analysis techniques, in order to improve the accuracy and validity of urban climate mapping to suit the micro-scale application. It is believed that this framework maintains the advantages in data visualization of previous UC-Map methods, while improves its accuracy and validity for urban and building design implication through empirical modeling and weighting, and thus has a good potential in climate-responsive design research and practice.

Acknowledgment

References

[1] T.R. Oke, The Boundary Layer Climates, 2nd edition, Methuen, London and New York, 1987.
[2] I.D. Stewart, T.R. Oke, E.S. Krayenhoff, Evaluation of the' local climate zones' scheme using temperature observations and model simulations, Int. J. Climatol. 33 (8) (2013) 1–19.
[3] Q. Chen, Using computational tools to factor wind into architectural environment design, Energy Build. 36 (2004) 1197–1209.
[4] L. Chen, E. Ng, X. An, C. Ren, M. Lee, U. Wang, et al., Sky view factor analysis of street canyons and its implications for daytime intra-urban air temperature differentials in high-rise, high-density urban areas of Hong Kong: a GIS-based simulation approach, Int. J. Climatol. 32 (1) (2012) 121–136.
[5] VDI., VDI-Guideline 3787, Part 1: Environmental Meteorology-Climate and Air Pollution Maps for Cities and Regions, Beuth Verlag, Berlin, 1997.
[6] TMG., The Thermal Environment Map and Areas Designated for the Implementation of Measures against the Heat Island Phenomenon, Bureau of Environment, Bureau of Urban Development, Tokyo Metropolitan Government (TMG), Tokyo, Japan, 2005.
[7] Planning Department Hong Kong SAR., Urban Climatic Map and Standards for Wind Environment—Feasibility Study—Final Report, Department of Architecture CUHK, Hong Kong, 2009.
[8] E. Ng, Towards planning and practical understanding of the need for meteorological and climatic information in the design of high-density cities: a case-based study of Hong Kong, Int. J. Climatol. 32 (4) (2012) 582–598.
[9] L. Chen, E. Ng, Quantitative urban climate mapping based on a geographical database: a simulation approach using Hong Kong as a case study, Int. J. Appl. Earth Obs. Geoinf. 13 (4) (2011) 586–594.
[10] F. Yang, S.S.Y. Lau, F. Qian, Urban design to lower summertime outdoor temperatures: an empirical study on high-rise housing in Shanghai, Build. Environ. 46 (3) (2011) 769–785.
[11] F. Yang, F. Qian, S.S.Y. Lau, Urban form and density as indicators for summertime outdoor ventilation potential: a case study on high-rise housing in shanghai, Build. Environ. 70 (2013) 122–137.
[12] Shanghai Municipal Statistics Bureau, Shanghai Statistical Yearbook 2014, China Statistical Press, Shanghai, 2015.
[13] T.R. Oke, Street design and urban canopy layer climate, Energy Build. 11 (1988) 103–113.
[14] C.S.B. Grimmond, T. Oke, Aerodynamic properties of urban areas derived from analysis of surface form, J. Appl. Meteorol. 38 (1998) 1262–1292.
[15] G.T. Johnson, I.D. Watson, The determination of view-factors in urban canyon, J. Clim. Appl. Meteorol. 23 (1984) 329–335.
[16] S.K. Jusuf, N.H. Wong, Development of empirical models for an estate level air temperature prediction in Singapore, Proceeding of Second International Conference on Countermeasures to Urban Heat Islands. Berkeley, California, USA (2009).
[17] A.K.L. Quah, M. Roth, Diurnal and weekly variation of anthropogenic heat emissions in a tropical city Singapore, Atmos. Environ. 46 (2012) 92–103.
[18] B.L. Ong, Green plot ratio: an ecological measure for architecture and urban planning, Landsc. Urban Plan. 63 (4) (2003) 197–211.
[19] S. Burian, Urban Informatics and Morphological Analysis, 2002.
[20] R. Giridharan, S.S.Y. Lau, S. Ganesan, B. Givoni, Urban design factors influencing heat island intensity in high-rise high-density environments of Hong Kong, Build. Environ. 42 (10) (2007) 3669–3684.
[21] Q.-Y. Zhang, H.-X. Yang, Typical Meteorological Database Handbook for Buildings, China Architecture and Building Press, Beijing, 2012.
[22] T.R. Oke, Canyon geometry and the nocturnal urban heat island: comparison of scale model and field observations, Int. J. Climatol. 1 (3) (1981) 237–254.
[23] F. Yang, S.S.Y. Lau, F. Qian, Summertime heat island intensities in three high-rise housing quarters in inner-city Shanghai China: building layout, density and greenery, Build. Environ. 45 (1) (2010) 115–134.
[24] L. Shashua-Bar, M. Hoffman, Quantitative evaluation of passive cooling of the ucl microclimate in hot regions in summer, case study: urban streets and courtyards with trees, Build. Environ. 39 (9) (2004) 1087–1099.
[25] E. Kruger, B. Givoni, Outdoor measurements and temperature comparisons of seven monitoring stations: preliminary studies in Curitiba, Brazil, Build. Environ. 42 (4) (2007) 1685–1698.
[26] P. Hoppe, The physiological equivalent temperature–a universal index for the biometeorological assessment of the thermal environment, Int. J. Biometeorol. 43 (1999) 71–75.
[27] T.-P. Lin, A. Matzarakis, R-L. Hwang, Shading effect on long-term outdoor thermal comfort, Build. Environ. 45 (1) (2010) 213–221.
[28] J. Niu, J. Liu, Lee T-c, Z. Lin, C. Mak, K.-T. Tse, et al., A new method to assess spatial variations of outdoor thermal comfort: onsite monitoring results and implications for precinct planning, Build. Environ. 91 (0) (2015) 263–270.
[29] ISO-7726., Ergonomics of the Thermal Environment—Instruments for Measuring Physical Quantities, ISO, Geneva, 1998.
[30] T. Gál, J. Unger, A new software tool for SVF calculations using building and tree-crown databases, Urban Clim. 10 (Part 3 (0)) (2014) 594–606.
[31] C.V. Gal, The influence of built form and vegeetation on the canopy layer microclimate within urban blocks, Acta Climatol. Chorol. Univ. Szeged. 47-48 (43-52) (2014).
[32] F. Lindberg, C.S.B. Grimmond, The influence of vegetation and building morphology on shadow patterns and mean radiant temperatures in urban areas: model development and evaluation, Theor. Appl. Climatol. 105 (3–4) (2011) 311–323.
[33] J.C. Hii, N.H. Wong, S.K. Jusuf, Anthropogenic heat contribution to air temperature increase at pedestrian height in Singapore's high density Central Business District (CBD), 9th International Conference on Urban Climate (ICUC9). Toulouse France, (2015) 1–6.
[34] A. Matzarakis, H. Mayer, M.G. Iziomon, Applications of a universal thermal index: physiological equivalent temperature, Int. J. Biometeorol. 43 (2) (1999) 76–84.